

**Figure 1.** Layer constituents and sample structure. The polycation used in the LBL growth is poly(diallyldimethylammonium chloride) (PDAC), and the anion is TDBC, a J-aggregate-forming cyanine dye. Optical measurements are taken with the LBL-film side of the sample facing the light beam at a specified angle  $\theta$  away from the normal.

plot of root-mean-square (RMS) roughness versus the number of SICAS steps.

As shown in the AFM images for 1.5 SICAS and 2.0 SICAS compared to blank glass, the layered structure of the PDAC/TDBC J-aggregate films does not appear until the second dye immersion. This delay is likely caused by the lack of a precursor layer or surface treatment on the glass support. The images show that layered growth is still dominant at 4.5 SICAS, but at 6.5 SICAS and 10.5 SICAS the growth has shifted to a Stransky–Krastranov (SK) type of process, forming large islands of material. To quantify the growth trend, RMS roughness was measured from  $16 \mu\text{m}^2$  AFM images of films that underwent 3.5 SICAS to 10.5 SICAS. The plot in Figure 2 shows that a mostly constant RMS roughness in the range of 1.4 to 2.0 nm persists through the first 5.5 SICAS, indicating layered growth, but beyond 6.5 SICAS, the roughness increases, indicating the shift to SK-type growth.

The thickness data obtained from the AFM measurements were combined with optical transmittance and reflectance data to extract the optical constants of the LBL PDAC/TDBC J-aggregate films. The plots in Figure 3 show the measured optical data and results of the analysis.

We model light propagation through the sample by using propagation and interface-matching matrices, with film thicknesses as inputs to the model, and refractive indices as fitting parameters. The implementation details of this model are described further in the Experimental section. Two methods are employed in calculating the  $(n,k)$  values. In the first method, the  $(n,k)$  values are obtained by minimizing the sum of least-squared errors of the calculated transmittance and reflectance for the first four sample thicknesses. This approach is similar to that described by Djurišić et al.,<sup>[4]</sup> however, in our method we perform a single  $(n,k)$  fit and do not incorporate the use of a penalty function in calculating the least-squared errors. In the first method, we assume that the absorption constant in the layered growth regime does not change as more PDAC/TDBC layers are deposited. The ranges in  $n$  and  $k$  values are

[0.05,5] and [0,6], respectively, with a resolution of 0.05 in both. It should be noted that since no PDAC/TDBC layer is evident for the first 1.5 SICAS, the transmittance and reflectance data for the first layer correspond to what we refer to as the 2.5 SICAS sample. Numerical fits to the thickness-dependent reflectance and transmittance data at wavelength  $\lambda = 596 \text{ nm}$  based on the first method are shown in Figure 3d for complex index of refraction with a real part,  $n$ , between 1.55 and 1.85, and an imaginary part,  $k$ , between 4.65 and 5.60. The high extinction coefficient,  $k$ , corresponds to an absorption constant of the film of  $\alpha = 4\pi k/\lambda = (1.05 \pm 0.1) \times 10^6 \text{ cm}^{-1}$  at  $\lambda = 596 \text{ nm}$ . In our analysis we assume complete layer coverage in contrast to the partial coverage observed in Figure 2. This assumption underestimates the  $k$  values for the thin film.

The second method employed in calculating the  $(n,k)$  values is based on the Kramers–Kronig (KK) transformations, which relate the real and imaginary parts of the index of refraction. The details of the KK regression are explained in the Experimental section. For samples that underwent 2.5 SICAS (estimated as one complete layer) to 5.5 SICAS (estimated as four complete layers), the  $(n,k)$  spectra for each sample are calculated from the sample's reflectance spectrum. Figures 3e–g show the results of the KK regressions. Figure 3e shows the measured transmittance and reflectance for the three-layer (5.1 nm thick) film along with the reflectance and transmittance calculated from the  $(n,k)$  spectra in Figure 3f. The transmittance calculated from the KK regression is in good agreement with the measured transmittance. Figure 3g shows the peak in  $k$  for one-layer (1.7 nm thick) to four-layer (6.8 nm thick) films calculated using the KK regressions, as well as the movement of the peak in  $k$  to lower energies as the number of layers increases. The results of the KK regression confirm the high magnitude of the absorption constant of the film found through the first method.

Several trends are noticeable in the optical data as samples undergo more SICAS. The reflectance data in Figure 3a show that the peak in reflectance moves to lower energy and that

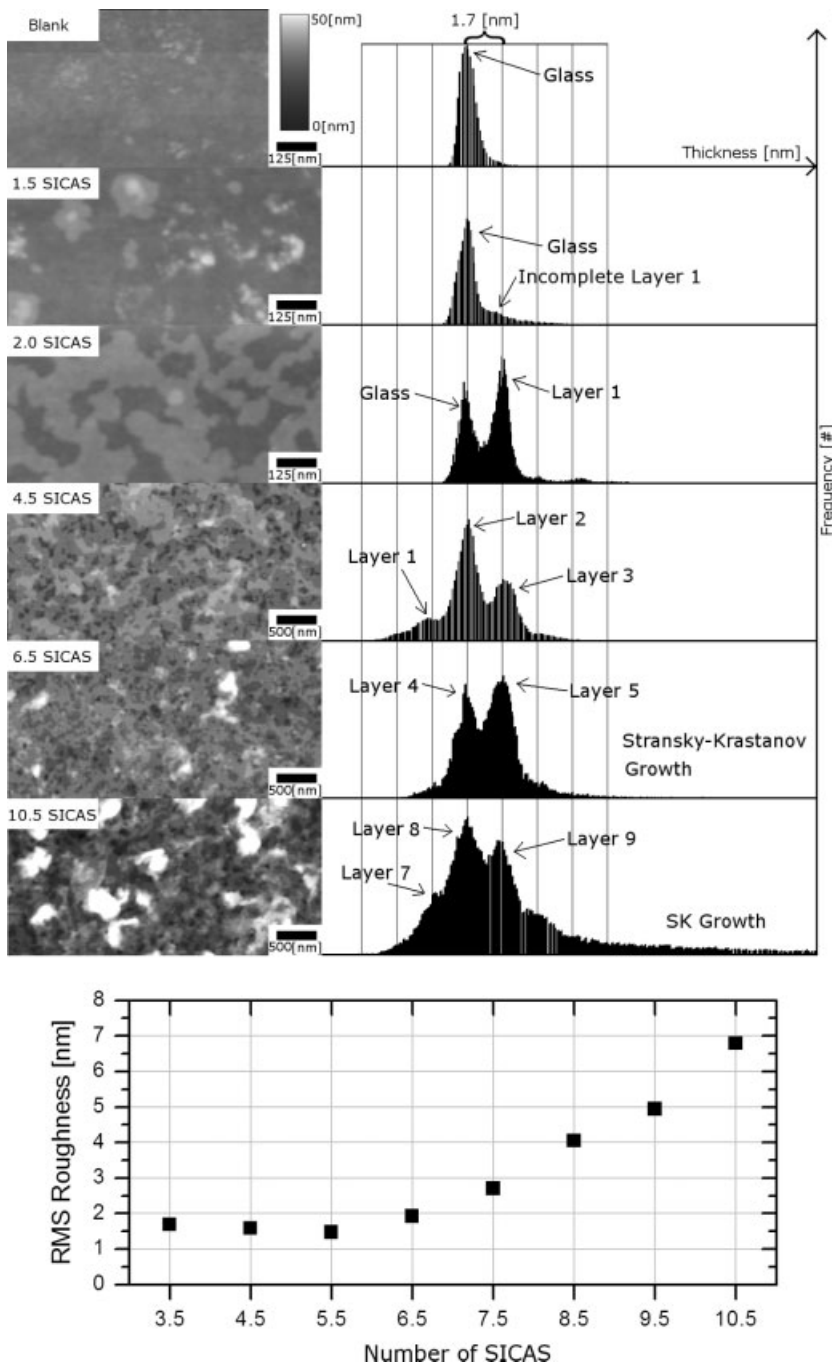


**Figure 2.** AFM images of LBL-assembled J-aggregate growth with histograms of thickness frequency. Each SICAS consists of a PDAC adsorption step followed by a TDBC adsorption step, with  $N.5$  SICAS referring to  $N$  SICAS steps followed by an additional PDAC adsorption step. The AFM images show samples that underwent the indicated number of SICAS. The top three images show that significant PDAC/TDBC layered growth is not evident until 2.0 SICAS. The bottom three images show the build up of thick layers. The histograms are lined up at the dominant film thicknesses to show that each layer is about 1.7 nm thick, the estimate used when modeling the optical constants of the films. The histograms are created from the full  $1 \mu\text{m}^2$  and  $16 \mu\text{m}^2$  images for the first three and last three films shown, respectively. The layer numbers indicated in the histograms are based on the progression of layer growth observed in AFM images. The plot shows the roughness profile of films from 3.5–10.5 SICAS. The roughness is nearly constant until 6.5 SICAS, when the dominant growth regime changes from layered to Stransky-Krastanov type. All images have a vertical scale of 50 nm.

the full width at half maximum (FWHM) increases. In addition, Figure 3c shows the onset of a high-energy peak in absorption. Lastly, the KK regression results plotted in Figure 3g show the peak  $k$  value increasing with the number of SICAS. We have considered two approaches in explaining these trends.

The first explanation is based on the changing morphology of the thin films. Our assumption of complete layer coverage in numerical analysis could be responsible for the apparent increase in  $k$  plotted in Figure 3g. In addition, the increase in reflectance FWHM may be due to a weak microcavity caused by SK growth or increasing inhomogeneous broadening. Lastly, the onset of the high-energy peak could be attributed to vibronic states in the J-aggregate, as noted in previous studies of J-aggregate monolayer films deposited using a Langmuir–Blodgett technique.<sup>[5]</sup>

An alternative explanation is based on strong coupling of the J-aggregate excitons to the electromagnetic field in the form of exciton–polaritons.<sup>[6]</sup> The effects of strong coupling will be more pronounced as the density of dipoles increases, resulting in a higher  $k$  for the films as more layers are added. Additionally, a larger reflectance FWHM will result from an increase in the splitting between the exciton–polariton longitudinal and transverse modes. Lastly, the high-energy peak in absorption could be attributed to the exciton–polariton longitudinal mode. The observed trend in Figure 3a of the peak in reflectance moving to lower energy is consistent with both explanations. A weak cavity effect resulting from SK growth may be responsible for the small shift in the peak reflectance to lower energy as the cavity thickness increases.

LBL-assembled thin films of PDAC/TDBC J-aggregates possess remarkable morphological and optical properties that make them well suited for use in strong coupling optoelectronic applications, enabling the creation of exciton–polariton optoelectronic devices that operate at room temperature.<sup>[1g]</sup> With LBL assembly, J-aggregates form nanometer-scale physical layers, allowing highly absorbing thin films to be assembled with precise control of thickness. Moreover, the high absorption constant of the PDAC/TDBC films,

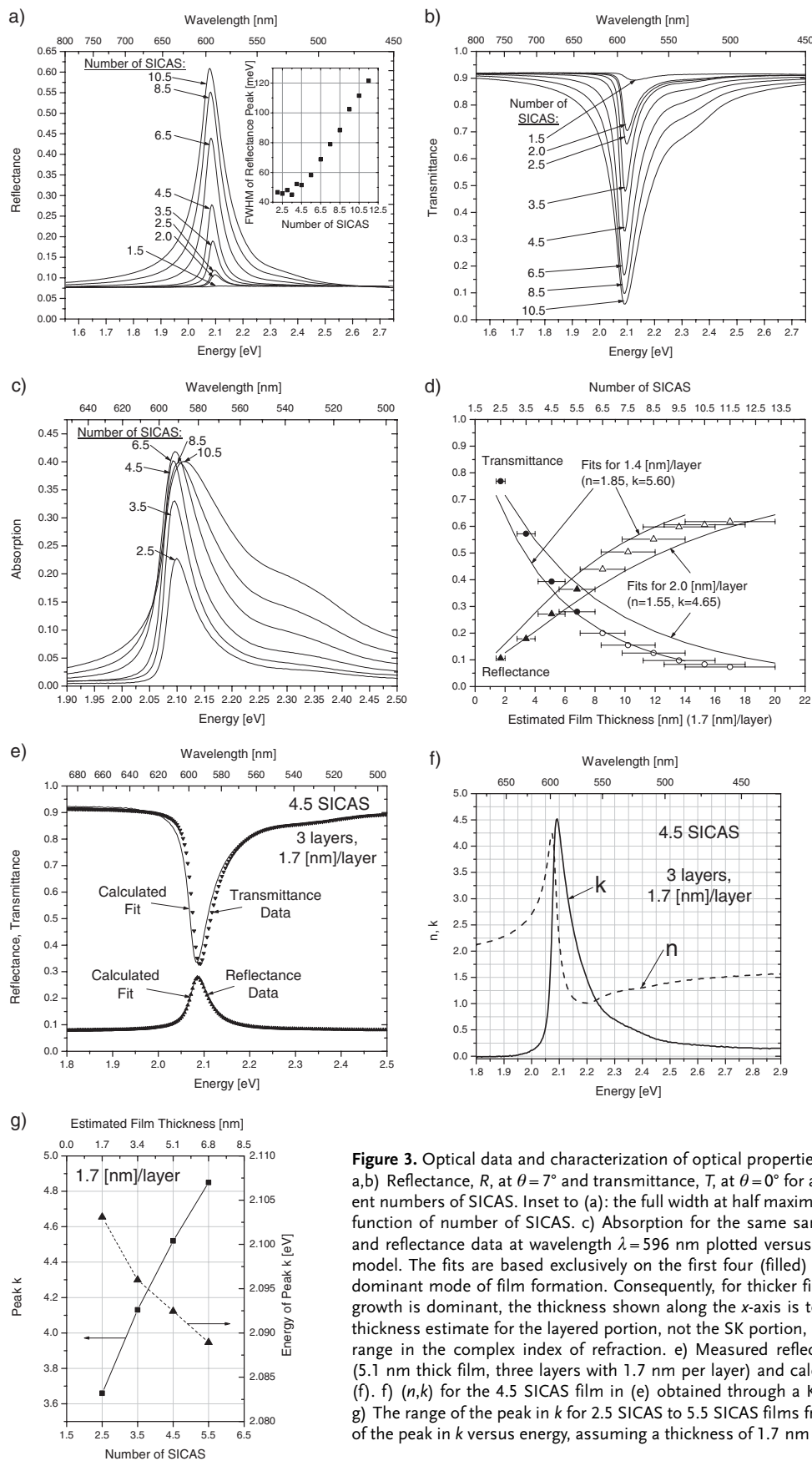


**Figure 3.** Optical data and characterization of optical properties for LBL PDAC/TDBC J-aggregate films. a,b) Reflectance,  $R$ , at  $\theta = 7^\circ$  and transmittance,  $T$ , at  $\theta = 0^\circ$  for a series of samples that underwent different numbers of SICAS. Inset to (a): the full width at half maximum (FWHM) of the reflectance peak as a function of number of SICAS. c) Absorption for the same samples given by 1– $R$ – $T$ . d) Transmittance and reflectance data at wavelength  $\lambda = 596$  nm plotted versus film thickness, along with fits from our model. The fits are based exclusively on the first four (filled) data points where layered growth is the dominant mode of film formation. Consequently, for thicker films (unfilled data points) where SK-type growth is dominant, the thickness shown along the x-axis is to be interpreted as the AFM-determined thickness estimate for the layered portion, not the SK portion, of the film. The two fits plotted show the range in the complex index of refraction. e) Measured reflectance and transmittance for 4.5 SICAS (5.1 nm thick film, three layers with 1.7 nm per layer) and calculated spectra using the  $(n, k)$  shown in (f). f)  $(n, k)$  for the 4.5 SICAS film in (e) obtained through a KK regression based on reflectance data. g) The range of the peak in  $k$  for 2.5 SICAS to 5.5 SICAS films from KK regression as well as the position of the peak in  $k$  versus energy, assuming a thickness of 1.7 nm per layer.

$\alpha = (1.05 \pm 0.1) \times 10^6 \text{ cm}^{-1}$  at  $\lambda = 596 \text{ nm}$ , is a lower limit, as even higher absorption-constant values could be obtained by developing full coverage of the substrate surface with similarly directed J-aggregate domains.

## Experimental

J-aggregate thin films were produced using layer-by-layer (LBL) assembly. Layers of polyelectrolyte and J-aggregate-forming dye were alternately adsorbed onto glass slides. The dye used was 5,6-dichloro-2-[3-[5,6-dichloro-1-ethyl-3-(3-sulfopropyl)-2(3H)-benzimidazolide]-1-propenyl]-1-ethyl-3-(3-sulfopropyl) benzimidazolium hydroxide, inner salt, sodium salt obtained from Nippon Kankoh Shikiso Kenkyusho Co., Ltd. (CAS 28272-54-0) (TDBC). The polyelectrolyte used was poly(diallyldimethylammonium chloride) (PDAC), 20 % by weight in water, weight-average molecular weight,  $M_w = 400\,000\text{--}500\,000$ , obtained from Sigma-Aldrich (CAS 26062-79-3). The dye solvent and rinses for the dye-adsorption step were approximately pH 9 solutions of deionized (DI) water plus sodium hydroxide. The effect of pH on TDBC has been documented [7]. The sodium hydroxide was obtained from EM Science. The polyelectrolyte solvent and rinses for the polyelectrolyte adsorption step were deionized (DI) water.

A standardized routine was used to prepare the dye and polyelectrolyte solutions. The dye solution was approximately  $5 \times 10^{-5} \text{ M}$ . Once the dye was added to the dye solvent, the dye bucket was placed in an ultrasonic cleaner to sonicate for 30 min. The dye was then mixed with a 1 in (2.54 cm) magnetic spin bar for 10 min, sonicated for 20 min, mixed for 5 min, and finally sonicated for 5 min. The polyelectrolyte solution was approximately  $3 \times 10^{-2} \text{ M}$ , prepared by adding 10 mL of polyelectrolyte to 390 mL of DI water. The polyelectrolyte solution was prepared using the same time intervals for mixing/sonication as the dye-solution preparation, except sonication and mixing at each step were swapped. Care was taken throughout the deposition to shield the dye solution and samples from light.

Prior to the deposition, the glass slides were cleaned with a detergent solution (Micro-90), acetone, and isopropanol. The acetone, isopropanol, and methanol used in this study were OmniSolv-brand solvents made by EMD Chemicals. The slides were then treated with oxygen plasma for six minutes in a Plasma Preen system. The LBL deposition was performed using an automated Leica Autostainer XL. The polyelectrolyte-adsorption step consisted of dipping the slides in polyelectrolyte solution for 15 min and in the three rinses for 2, 2, and 1 min, respectively. The dye-adsorption step used the same time intervals as those used in the polyelectrolyte adsorption step.

Upon removal from the stainer, each sample was blown dry using nitrogen gas. For each sample, the sample face that was not treated with oxygen plasma prior to deposition was cleaned using methanol to remove deposited layers.

Measurements for this study were performed in the MIT Center for Materials Science and Engineering Shared Analytical Lab. The atomic force microscopy (AFM) data were collected on a Digital Instruments D3000 Scanning Probe Microscope in tapping mode using phosphorus-doped silicon tips from Veeco. The optical data were collected using a Cary 5E UV-vis-NIR spectrophotometer. The transmission data were collected with the light beam at normal incidence,  $\theta = 0^\circ$ . The reflectance data were collected in a V-W setup with the light beam incidence at  $\theta = 7^\circ$  using the Cary Specular Reflectance Accessory in Absolute Reflectivity mode.

For numerical calculations, we modeled the films using propagation and matching matrices: [8]

$$\begin{bmatrix} E_{1a}^+ \\ E_{1a}^- \end{bmatrix} = \begin{bmatrix} e^{-i\beta} & 0 \\ 0 & e^{i\beta} \end{bmatrix} \begin{bmatrix} E_{1b}^+ \\ E_{1b}^- \end{bmatrix} \quad (1)$$

$$\begin{bmatrix} E_{1b}^+ \\ E_{1b}^- \end{bmatrix} = \frac{1}{t} \begin{bmatrix} 1 & r \\ r & 1 \end{bmatrix} \begin{bmatrix} E_{2b}^+ \\ E_{2b}^- \end{bmatrix} \quad (2)$$

Equation 1 shows a propagation matrix equation, which relates the forward and reverse traveling electric field amplitudes at boundary  $a$  to the amplitudes at boundary  $b$ . The medium (1) is modeled by the parameter  $\beta = 2\pi\tilde{n}d/\lambda$ , where  $\tilde{n}$  is the complex index of refraction of the medium,  $\tilde{n} = n + ik$ , and  $d$  is the thickness of the layer. Equation 2 shows a matching matrix equation, which matches the forward- and reverse-traveling electric-field amplitudes at boundary  $b$ .  $r$  and  $t$  are, respectively, the reflection and transmission Fresnel coefficients for a wave incident from medium 1 to medium 2. The parameters  $\beta$ ,  $r$ , and  $t$  must be modified slightly to model non-normal incidence [8]. Our model calculated transmittance at  $\theta = 0^\circ$  and reflectance at  $\theta = 7^\circ$  based on the light traveling through air ( $\tilde{n} = 1$ ), an LBL PDAC/TDBC J-aggregate film, the glass slide ( $\tilde{n} = 1.5$ ), and then air ( $\tilde{n} = 1$ ). From the AFM data, the thickness of deposited physical layers was observed to vary from about 1.4 to 2.0 nm per adsorbed layer. Because the glass-substrate thickness,  $d_s$ , is very large in the wavelength range of interest ( $d_s/\lambda \gg 1$ ), we modeled the glass as 1 mm thick and averaged the calculated transmittance and reflectance for ten glass-thickness variations comprising a phase change of 0 to  $2\pi$  at the wavelength of interest in order to remove interference effects in the substrate. For near-normal incidence calculations, the light from the spectrometer was assumed to be circularly polarized.

The Kramers–Kronig (KK) regressions for finding  $(n, k)$  were based on the method outlined by Nitsche and Fritz [9]. The propagation and matching matrix model described above was used to calculate the reflectances and transmittances used in the KK regression. However, to minimize convergence errors introduced by interference in the substrate, we used one-hundred glass variations comprising a phase change of 0 to  $2\pi$  at the wavelength of interest. We used the following approximation of the KK transformation given by Nitsche and Fritz relating  $n$  and  $k$ :

$$n(\omega_j) \cong n_{\text{offset}} + \frac{2}{\pi} P \int_{\omega_L}^{\omega_U} \frac{\omega k(\omega)}{\omega^2 - \omega_j^2} d\omega, \quad \omega_L \leq \omega_j \leq \omega_U \quad (3)$$

The background contributions of frequencies outside of the measured spectrum are approximated through the use of the  $n_{\text{offset}}$  term in Equation 3. For our regressions, we used  $n_{\text{offset}} = 1.7$  since we assume that PDAC and TDBC resemble many other organic materials outside of the visible spectrum. Like Nitsche and Fritz, we implemented a Levenberg–Marquardt algorithm for use in optimizing  $k$  [10]. Our maximum step size at each iteration was 0.01, which ultimately dictated the resolution of the resulting  $k$  spectra. The Cauchy principal value in Equation 3 was approximated using Maclaurin's formula [11].

Received: January 31, 2005  
Final version: March 16, 2005

- [1] a) E. E. Jelley, *Nature* **1936**, 138, 1009. b) C. Weisbuch, M. Nishioka, A. Ishikawa, Y. Arakawa, *Phys. Rev. Lett.* **1992**, 69, 3314. c) D. G. Lidzey, D. D. C. Bradley, M. S. Skolnick, T. Virgili, S. Walker, D. M. Whittaker, *Nature* **1998**, 395, 53. d) D. G. Lidzey, D. D. C. Bradley, T. Virgili, A. Armitage, M. S. Skolnick, S. Walker, *Phys. Rev. Lett.* **1999**, 82, 3316. e) P. Schouwink, H. V. Berlepsch, L. Dahne, R. F. Mahrt, *Chem. Phys. Lett.* **2001**, 344, 352. f) C. Weisbuch, H. Benisty, R. Houdre, *J. Lumin.* **2000**, 85, 271.
- [2] a) G. Decher, J. D. Hong, J. Schmitt, *Thin Solid Films* **1992**, 210–211, 831. b) K. Ariga, Y. Lvov, T. Kunitake, *J. Am. Chem. Soc.* **1997**, 119, 2224. c) H. Fukumoto, Y. Yonezawa, *Thin Solid Films* **1998**, 327–329, 748. d) E. Rousseau, M. Van der Auweraer, F. C. De Schryver, *Langmuir* **2000**, 16, 8865. e) E. Rousseau, M. M. Koetse, M. Van der Auweraer, F. C. De Schryver, *Photochem. Photobiol. Sci.* **2002**, 1, 395. f) A. Naber, U. C. Fischer, S. Kirchner, T. Dziomba, G. Kollar, L. F. Chi, H. Fuchs, *J. Phys. Chem. B* **1999**, 103, 2709. g) C. Peyratout, L. Dahne, *Phys. Chem. Chem. Phys.* **2002**, 4, 3032. h) M. Kawasaki, T. Sato, T. Yoshimoto, *Langmuir* **2000**, 16, 5409.

- [3] E. G. Bortchagovsky, U. C. Fischer, *Appl. Opt.* **2003**, *42*, 6915.  
 [4] A. B. Djuricic, T. Fritz, K. Leo, E. H. Li, *Appl. Opt.* **2000**, *39*, 1174.  
 [5] a) M. Orrit, D. Möbius, U. Lehmann, H. Meyer, *J. Chem. Phys.* **1986**, *85*, 4966. b) H. Kuhn, D. Möbius, H. Bücher, in *Physical Methods of Chemistry: Part IIIB Optical, Spectroscopic, and Radioactivity Methods* (Eds: A. Weissberger, B. Rossiter), Wiley-Interscience, New York **1972**, p. 577.  
 [6] a) L. Dahne, A. Horvath, G. Weiser, *Chem. Phys.* **1993**, *178*, 449. b) M. Vacha, M. Saeki, M. Furuki, L. S. Pu, K.-I. Hashizume, T. Tani, *J. Lumin.* **2002**, *98*, 35. c) R. Stepniewski, K. P. Korona, A. Wyszomle, J. M. Baranowski, K. Pakula, M. Potemski, G. Martinez, I. Grzegory, S. Porowski, *Phys. Rev. B* **1997**, *56*, 15 151. d) R. N. Philp, D. R. Tilley, *Phys. Rev. B* **1991**, *44*, 8170. e) R. N. Philp, D. R. Tilley, *Phys. Rev. B* **1991**, *44*, 8170. f) J. J. Hopfield, *Phys. Rev.* **1958**, *112*, 1555.  
 [7] I. A. Struganova, H. Lim, S. A. Morgan, *J. Phys. Chem. B* **2002**, *106*, 11 047.  
 [8] L. Ward, *The Optical Constants of Bulk Materials and Films*, IOP Publishing Ltd., Bristol, UK **1994**, p. 177.  
 [9] R. Nitsche, T. Fritz, *Phys. Rev. B* **2004**, *70*, 195 432.  
 [10] D. W. Marquardt, *J. Soc. Ind. Appl. Math.* **1963**, *11*, 431.  
 [11] K. Ohta, H. Ishida, *Appl. Spectrosc.* **1988**, *42*, 952.

## Control of Uniaxial Orientation and Fabrication of a Submicrometer-Sized, Oriented Structure in a Photocrosslinkable-Polymer Liquid-Crystalline Film\*\*

By Nobuhiro Kawatsuki,\* Takeshi Tachibana, and Kenji Kamada\*

Because of the development of new applications in nanophotonics, including ultra-high density information storage and the fabrication of three-dimensional (3D) microstructures, two-photon absorption (TPA) in organic materials has been eagerly investigated.<sup>[1–5]</sup> In TPA, intense laser pulses are used to excite molecules through a virtual state with photons that have half the nominal one-photon excitation energy. Special selection of the target by using a tightly focused fem-

tosecond (fs) laser creates a micro-3D structure, since the probability of TPA depends on the intensity of the laser pulse and is typically based on an isotropic two-photon reaction.<sup>[2,3,6]</sup> When a fs-pulse laser is linearly polarized (LP), an axis-selective photoreaction that induces an anisotropic two-photon reaction is possible. A few studies have reported an axis-selective two-photon reaction using LP fs-pulse lasers.<sup>[7–9]</sup> Sekkat et al. demonstrated that two-photon photoisomerization and orientation of a diarylethene in a poly(methyl methacrylate) (PMMA) film generates a very small optical anisotropy of the dye molecules.<sup>[7]</sup> The same group recently reported polarization storage in an azobenzene-containing PMMA film using orientational hole burning, where the image exhibits polarization.<sup>[9]</sup> However, large molecular reorientation in polymeric films generated by two-photon irradiation has yet to be reported. Combining TPA and molecular reorientation should create a microstructure with 3D molecular orientation in polymeric films.

Large photoinduced molecular orientation has been investigated in photoreactive polymeric films that contain azobenzene or photocrosslinkable side groups.<sup>[10–14]</sup> It has been found that exposing an azobenzene-containing film to LP light induces axis-selective photoisomerization and subsequent reorientation of the azobenzene groups.<sup>[10–12]</sup> Alternatively, we have previously reported thermally enhanced photoinduced reorientation in a photocrosslinkable polymer liquid crystal (PMCB6M, Fig. 1) using linearly polarized UV (LPUV) light.<sup>[13,14]</sup> It was found that the direction of the in-

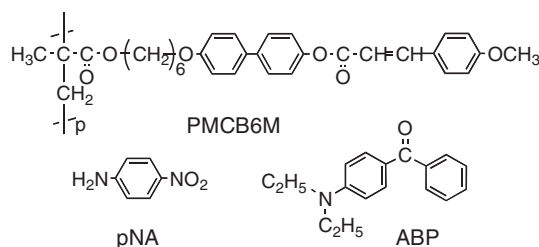


**Figure 1.** Chemical structures of PMCB6M and triplet sensitizers *p*-nitroaniline (pNA) and 4-(*N,N*-diethylamino)benzophenone (ABP).

plane molecular orientation could be regulated parallel to the polarization of the LPUV light and that the induced birefringence exhibited high thermal stability.<sup>[13]</sup> The photoreactivity for molecular reorientation in PMCB6M was vastly improved when the film contained a small amount of a triplet photosensitizer, such as a benzophenone derivative. The improvement came about by means of a polarization-selective triplet energy transfer from the excited photosensitizer to the mesogenic groups.<sup>[15]</sup> However, the thermally enhanced reorientational order with the photosensitizer was lower than without the photosensitizer.

It is known that *p*-nitroaniline (pNA) and benzophenone derivatives act as triplet photosensitizers for cinnamate derivatives<sup>[16]</sup> and as two-photon absorbing agents.<sup>[17,18]</sup> The TPA

[\*] Prof. N. Kawatsuki, T. Tachibana  
 Department of Materials Science and Chemistry  
 Himeji Institute of Technology, University of Hyogo  
 2167 Shosha Himeji, 671-2201 (Japan)  
 E-mail: kawatsuki@eng.u-hyogo.ac.jp  
 Dr. K. Kamada  
 Photonics Research Institute  
 National Institute of Advanced Industrial Science  
 and Technology, AIST  
 Kansai Center  
 1-8-31 Midorigaoka, Ikeda 563-8577 (Japan)  
 E-mail: k.kamada@aist.go.jp

[\*\*] This work was supported by a Grant-in-Aid for Scientific Research from the JSPS (15550187).